Supporting Information

Nanoplasmonic Quantitative Detection of Intact Viruses from Unprocessed Whole Blood

Fatih Inci [a, #], *Onur Tokel* [a, #], *ShuQi Wang* [a], *Umut Atakan Gurkan* [a], *Savas Tasoglu* [a], *Daniel R. Kuritzkes* [b], *and Utkan Demirci* [a,b,c *]

[a] Demirci Bio-Acoustic-MEMS in Medicine (BAMM) Laboratory, Division of Biomedical Engineering, Department of Medicine, Brigham and Women's Hospital, Harvard Medical School, Boston, MA 02139, USA.

[b] Division of Infectious Diseases, Brigham and Women's Hospital, Harvard Medical School, Boston, MA 02115, USA.

[c] Harvard-MIT Health Sciences and Technology, Cambridge, MA 02139, USA.

[#] Authors contributed equally

[*]Corresponding author: Utkan Demirci, PhD

Bio-Acoustic-MEMS in Medicine (BAMM) Laboratory,

Harvard-MIT Health Sciences and Technology

65 Landsdowne St., # 267

Cambridge, MA 02139, USA

Email: udemirci@rics.bwh.harvard.edu

MATERIALS AND METHODS

Materials. Ethanol (200 proof) was purchased from Fisher Scientific (Product no: E7023) (Fair Lawn, NJ). Phosphate buffered saline (PBS, pH = 7.4, 1×) was purchased from Invitrogen Co. (Product no: 10010) (Carlsbad, CA). Polystyrene well plates were purchased from Corning Inc. (Product no: 3997) (Corning, NY). 11-Mercaptoundecanoic acid (MUA), N-Ethyl-N'-(3-dimethylaminopropyl) carbodiimide hydrochloride (EDC), N-hydroxysulfosuccinimide (NHS) and bovine serum albumin (BSA, 10%) were obtained from Aldrich Chemical Co. (Product no: 450561, E6383, 56485, and A1595, respectively) (Milwaukee, WI). MES and poly-l-lysine (PLL) hydrobromide with 70,000-150,000 of molecular weight were purchased from Sigma Co. (Product no: M3671 and P1274, respectively) (St. Louis, MO). Gold nanoparticles with 10 nm diameter were purchased from TedPella (Product no: 15703) (Redding, CA) (Supplier Datasheet). NeutrAvidin™ protein was obtained from Pierce Biotechnology (Product no: 31000) (Rockford, IL). Biotinylated goat anti-HIV gp120 polyclonal antibody was obtained from Abcam Inc. (Product no: ab53937) (Cambridge, MA).

Surface modifications. Polystyrene surfaces were first washed with absolute ethanol and distilled water, then dried under nitrogen gas. Following cleaning steps, polystyrene surface was modified by PLL to form amine-terminated groups. A series of densities of PLL (from 0.01 to 0.1 mg/mL) in 1x PBS were evaluated, and then, surfaces were incubated at 4°C overnight. After PLL modification, 40 µL of gold nanoparticle solution was loaded onto each surface and incubated at 4°C overnight for binding and seeding of nanoparticles onto the support material. To evaluate gold nanoparticle binding and seeding on polystyrene surface, a series of poly-l-lysine (PLL) concentrations (0.01 to 0.1 mg/mL) were evaluated and a linear concentration-dependent wavelength shift was observed (Figure S1a). As we were preparing the surfaces to evaluate gold nanoparticle incubation time on amine-terminated polystyrene surface, we performed 1-day and 3-day incubation steps (Figure S1a). We observed a statistically comparable correlation between wavelength shift and PLL concentration for 1-day and 3-

day incubation steps (Figure S1a). Hence, we continued to perform the experiments using 1-day incubation of PLL to decrease the incubation time for the preparation of the devices. The individual wavelength of bare gold nanoparticles shifted from 519 nm to 545.5 ± 0.8 nm, when PLL concentration (1-day incubation) was increased from 0.01 to 0.1 mg/mL (Figure S1a). The number of amine groups played a crucial role in nanoparticle binding onto the surface.[1] On the other hand, higher PLL concentration (*i.e.,* 0.1 mg/mL) caused a collapsed polymer formation on the substrate, and a further increase in the concentration of gold nanoparticle binding sites on the surface was not observed (Figure S1b).

Antibody immobilization. We first activated gold nanoparticle immobilized surface with 100 μL of 1 mM MUA dissolved in ethanol. MUA forms carboxyl groups for crosslinking agents. EDC (100 mM EDC dissolved in 50 mM MES buffer at pH 5.0) reacts with carboxyl groups to form amine reactive intermediate. EDC-mediated coupling was stabilized by the addition of NHS (50 mM NHS dissolved in 50 mM MES buffer at pH 5.0). After EDC/NHS coupling reaction, 100 μL of NeutrAvidin (0.1 mg/mL) was placed on the modified support surface to immobilize antibodies on the surface and enhance the capture efficiency. [2] To minimize nonspecific binding on both inactive and reactive areas of the surface, 100 μL of 10% BSA was used as a blocking agent on each surface and incubated at 4°C for an hour. After the BSA blocking step, 5 μg/mL of biotinylated anti-gp120 polyclonal antibody was placed onto biotin binding sites on NeutrAvidin by loading 100 μL of antibody solution onto each modified surface and incubated at 4°C for an hour.

HIV Culturing. HIV-1 subtypes A, B, C, D, E, G, and a panel subtype, which consists of 6 major globally prevalent strains of genetically and biologically characterized HIV-1 isolates (A, B, C, D, and circulating recombinant forms (CRF01_AE and CRF02_AG)), were obtained from National Institutes of Health (NIH) under AIDS Research and Reference Reagent Program. The catalog number of panel is

11259 at NIH AIDS Research and Reference Reagent Program. These subtypes were collected from clinical samples in the United States and Uganda, and cultured in peripheral blood mononuclear cells (PBMCs) using a standard co-culture protocol. Briefly, HIV-1 negative PBMCs were first extracted using Ficoll Hypaque density gradient centrifugation (Histopaque 1077 Sigma H8889). After 3-day phytohemagglutinin (PHA) stimulation (0.25 μg /mL), HIV-1 negative PBMCs were co-cultured with HIV-1 infected PBMCs in R20/IL-2 (100 U/mL), which consists of RPMI-1640 (Cellgro® Mediatech 10-040-CV) implemented with L-Glutamine (300 mg/mL), 20% heat inactivated fetal bovine serum (FBS; Gemini), penicillin (50 U/mL), streptomycin (50 μg/mL), HEPES buffer (10 mM), and recombinant human interleukin-2 (100 U/mL, Roche). The culture was incubated under humidified 5% CO_2 atmosphere at 37 ºC, and culture supernatants were replaced bi-weekly with fresh medium. 3-day PHA stimulated HIV-1 infected PBMCs were added once a week and supernatants were collected for p24 testing (Perkin Elmer®, NEK050b). Culture termination was determined by p24 levels (at least 20 ng/mL) in cell-free supernatant, and virus supernatants were stored at -80 ºC for the quantification and sampling assays.

Quantification of HIV subtypes by reverse transcription-quantitative polymerase chain reaction (RT-qPCR) and sampling. Multiple HIV subtypes (A, B, C, D, E, G, and panel) were obtained from NIH under AIDS Research and Reference Reagent Program and cultured in peripheral blood mononuclear cells. Patient samples were obtained from Massachusetts General Hospital, Boston, MA and tested with the detection platform. To spike HIV in whole blood, HIV subtypes were first quantified by RT-qPCR (Roche COBAS®, Branchburg, NJ). We measured HIV concentrations diluted to 6.55 x 10^8, 6.37 x 10^8, 2.09 x 10^9, 7 x 10^8, 8.39 x 10^8, 6.53 x 10^8 and 1.48 x 10^9 copies/mL for subtypes A, B, C, D, E, G and panel (a mixture of different HIV subtypes[3]), respectively. For HIV stock sample quantification, viruses were lysed using guanidine isothiocyanate provided in the QIAamp Viral RNA Mini Kit (Qiagen, Valencia, CA), and then HIV RNA was extracted according to manufacturer's

instructions. To quantify HIV RNA, RT-qPCR was performed. For reverse transcription of HIV RNA samples, 10 µL of 2x core RT buffer, 2 µL of 10 µM of reverse primer (5'-GTCTGAGGGATCTCTCTAGTTACCAG-3'), 0.5 µL of AffinityScript (Applied Biosystems, Carlsbad, CA), and 7.5 µL of HIV RNA were used and performed on GeneAmp PCR System 9700 (Applied Biosystems, Carlsbad, CA). The reaction was set up to 25 °C for 5 minute, 45 °C for 60 minute and 95 °C for 3 minute incubation. For quantification of RNA, 50 µL of the master mixture was applied. Master mixture includes 1x core PCR buffer, 0.4 µM of forward primer LTR-F (5'-TAAAGCTTGCCTTGAGTGCT-3'), reverse primer LTR-R2, 0.2 µM of TaqMan probe LTR-P (5'-AGTAGTGTGTGCCCGTCTGTTGTGTG-3'), 2.5 units of SureStart Taq polymerase, and 10 µL of cDNA template. For the amplification step, 7300 Real-Time PCR System (Applied Biosystems, Carlsbad, CA) was first set up to 25 °C for 5 minutes and 95 °C for 10 minutes, and then, 50 cycles of 60 °C for a minute, and 95 °C for 30 seconds were performed. Following the viral load quantification, HIV stock solutions of A, B, C, D, E, G, and panel subtypes were spiked into unprocessed whole blood for the final concentration varying from 50 copies/mL to 1 x 10^6 copies/mL. 100 µL of spiked whole blood was loaded into each antibody immobilized surface by pipetting and incubated at 4°C for an hour. Whole blood samples without HIV spiking were used as controls (Figure 2). Following each surface modification and HIV sampling step, the surfaces were rinsed with 1x PBS three times, and 100 µL of PBS was then added to the wells for the spectral measurements. Each HIV data was subtracted from its own control spectra, which was measured before HIV sampling, and the resulting shift was presented as wavelength and extinction intensity change ± standard error of the mean (SEM). A second set of RT-qPCR was performed to minimize dilution inaccuracies. Same quantification protocol was utilized for discarded HIV patient samples. Before HIV detection, bound viruses were immobilized by a fixation solution containing paraformaldehyde and incubated at 4°C for an hour. Same sampling procedure was applied for HIV spiked (subtype panel) in PBS samples, and the results were presented in Figure S5. Since the lowest detection limit of RT-qPCR was set to 50 copies/mL, the results below 50 copies/mL

were reported as ~50 copies/mL (*e.g.,* 22 ± 20 copies/mL in HIV subtype A, 44 ± 11 copies/mL in HIV subtype C and 57 ± 17 copies/mL in HIV subtype E) and plotted with the original data point in the wavelength and extinction intensity shift figures.

Surface characterization and analysis by Atomic Force Microscopy. The formation of PLL coating and morphology of gold nanoparticles bound to polystyrene surfaces were characterized by using Atomic Force Microscopy (AFM) with scan areas of 5 μm x 5 μm. To evaluate the samples, polystyrene surfaces were first coated by PLL. Then, gold nanoparticles were incubated to immobilize them onto the PLL modified surfaces. After PLL and gold nanoparticle binding, the surface roughness change was evaluated by Asylum-1 MFP-3D AFM System (Asylum Research Inc., Santa Barbara, CA) under tapping mode using a 9 ± 2 nm AFM tip with a scan rate of 0.5 Hz. Five random 5 μm x 5 μm areas on biosensing surfaces were evaluated. Root mean square (RMS) roughness measurements were further statistically analyzed using non-parametric Kruskal-Wallis one-way analysis of variance followed by Mann-Whitney U test with Bonferroni correction, where statistical significance threshold was set to 0.05. We further evaluated gold nanoparticle immobilization and binding on PLL modified surfaces. We measured that gold nanoparticles bound sequentially onto the modified surface forming active areas of 18.97 ± 1.34 nm in height.

Scanning Electron Microscopy imaging of the captured virus. Polystyrene surfaces with 4 x 10^6 μm^2 were used to evaluate the capture of HIV samples from whole blood. After antibody immobilization on the biosensing platform, polystyrene surfaces that captured HIV from whole blood (10^6 copies/mL) was cut by a glass cutter, and then, prepared for Scanning Electron Microscopy (SEM) imaging. SEM images were taken at 4.7 mm working distance and 4.00 kV accelerating voltage in the presented figure.

Theoretical modeling of capture efficiency: To evaluate the number of gold nanoparticles on the

active area, we defined and used the following equations[4]:

$$N = V \times C \times \frac{A_b}{A} \times P \times \frac{R^2}{r^2}$$

$$P = \pi {r_0}^2 \exp\left\{-\frac{\lambda}{k_b T}\left[6(a\gamma^{-1} + \delta_{eq})F^s + 8\frac{a^2}{r_0}T^s\right] \times \frac{a}{{r_0}^2}\frac{\mu S}{m_r}\right\}(m_r m_l {K_a}^0)$$

$$F^s = 1 + (1.736 - 0.138\gamma + 0.128\gamma^2 + 0.09\gamma^3)e^{-\gamma}$$

$$T^s = 1 + (-20.50 - 46.50\gamma - 35.10\gamma^2 + 8.95\gamma^3)e^{-\gamma}$$

where N is the number of gold nanoparticles on active area, V is the volume of virus solution (mL), C is the number of copies of viruses per mL, A_b is the optical beam area (mm^2), A is whole surface area (μm^2), P is the capture efficiency of viruses, and R^2/r^2 is the surface area ratios of a virus and gold nanoparticle. Here, m_r and m_l are the receptor and ligand densities, respectively; ${K_a}^0$ is the association constant at zero load of the ligand-receptor pair; μS is the shear stress at the wall, F^s and T^s are shape-dependent coefficients; λ is the characteristic length of the ligand-receptor bonds; k_b is the Boltzmann constant; a is half-length of major axis of virus; δ_{eq} is the equilibrium separation distance between the virus and the surface; r_0 is the radius of the circular section of a virus located at a separation distance h_o from the surface; γ is the virus aspect ratio ($=a/b = 1$); and T is the temperature. m_l and ${K_a}^0$ are not known for viruses, to the best of our knowledge. The capture probability increases as the surface density of the receptors m_r and surface density of the ligands m_l increases, and as the affinity constant ${K_a}^0$ grows.

Our earlier results demonstrated 69.7 to 78.3% capture efficiency for HIV spiked in whole blood samples using anti-gp120 polyclonal antibody in a microfluidic chips.[2] Both the earlier system and the current system are incubation based, therefore we assume virus particles find enough time to get

sufficiently close to the surface in both experiments. Based on these results, here we assume 70% capture efficiency of viruses in multi-well plates. Note that, for a more detailed estimate of the capture efficiency, one has to calculate the probabilities of viruses to be located close to a surface (where capture occurs) and incorporate this probability into estimations. By using these equations, and substituting the values given in Table S5, we estimated the number of gold nanoparticles in contact with viruses in the active area, and plotted in Figure S4.

Results of experimental data maximum method. In the presence of HIV subtype A, the highest peak shift was observed at 5.2 ± 0.5 nm at (6.5 ± 0.6) x 10^5 copies/mL (Figure S6a). The detected peak shift decreased with decreasing viral concentration. For instance, down to 50 copies/mL HIV viral load resulted in a change of 1.3 ± 0.5 nm (Figure S6a). In the presence of HIV subtype B, the highest ((8.3 ± 1.3) x 10^5 copies/mL) and lowest (89 ± 6 copies/mL) concentrations of HIV viral load resulted in 4.7 ± 0.5 nm and 2.5 ± 0.8 nm peak shifts, respectively (Figure S6b). HIV subtype C spiked in blood samples displayed a peak shift of 6.3 ± 0.9 nm at (1.3 ± 0.2) x 10^6 copies/mL concentration, and 2.7 ± 0.9 nm shift at ~50 copies/mL concentration (Figure S6c). In the presence of HIV subtype D, the wavelength shifted by 4.3 ± 0.5 nm at (3.8 ± 1.2) x 10^6 copies/mL concentration, and by 1.7 ± 0.5 nm at 98 ± 39 copies/mL concentration (Figure S6d). HIV subtype E spiked in blood samples displayed a peak shift of 4.7 ± 0.8 nm at (1.3 ± 0.2) x 10^6 copies/mL concentration, and 1.2 ± 0.8 nm shift at ~50 copies/mL concentration (Figure S6e). In the presence of HIV subtype G, the highest peak shift was observed to be 4.8 ± 0.9 nm at (1.1 ± 0.3) x 10^6 copies/mL (Figure S6f). The peak shift for 404 ± 54 copies/mL HIV viral load was 2.0 ± 0.7 nm (Figure S6f). In the presence of HIV subtype panel, the highest peak shift was observed to be 6.5 ± 0.8 nm at (2.9 ± 0.5) x 10^6 copies/mL (Figure S6g). The peak shift for 245 ± 101 copies/mL HIV viral load was 1.5 ± 0.5 nm (Figure S6g). We also validated HIV viral load using 8 HIV-infected anonymous discarded patient whole blood samples using the nanoplasmonic platform. In the presence of discarded patient samples, the highest peak shift was observed to be 2.8 ± 0.5 nm at

3910 ± 400 copies/mL (Figure S6h). The peak shift for 481 ± 73 copies/mL HIV viral load was 1.3 ± 0.6 nm (Figure S6h).

Repeatability of the biosensing platform. To evaluate the repeatability of the biosensing platform technology, we defined an equation as follows:

$$Repeatability = \frac{Mean\ of\ WS\ per\ concentration}{Mean\ of\ WS\ per\ concentration + SEM\ per\ concentration}\ x\ 100$$

where WS is wavelength shift, and SEM is the standard error of the mean (SEM). In HIV subtype A spiked samples, the repeatability was observed to be 73 – 91% at the corresponding concentrations ranging from ~50 copies/mL to (6.5 ± 0.6) x 10^5 copies/mL. In HIV subtype B spiked samples, the repeatability was observed to be 75 – 90% at the corresponding concentrations ranging from 89 ± 6 copies/mL to (8.3 ± 1.3) x 10^5 copies/mL. In HIV subtype C spiked samples, the repeatability was observed to be 75 – 88% at the corresponding concentrations ranging from ~50 copies/mL to (1.3 ± 0.2) x 10^6 copies/mL. In HIV subtype D spiked samples, the repeatability was observed to be 64 – 90% at the corresponding concentrations ranging from 98 ± 39 copies/mL to (3.8 ± 1.2) x 10^6 copies/mL. In HIV subtype E spiked samples, the repeatability was observed to be 59 – 85% at the corresponding concentrations ranging from ~50 copies/mL to (1.3 ± 0.2) x 10^6 copies/mL. In HIV subtype G spiked samples, the repeatability was observed to be 75 – 84% at the corresponding concentrations ranging from 404 ± 54 copies/mL to (1.1 ± 0.3) x 10^6 copies/mL. In HIV subtype panel spiked samples, the repeatability was observed to be 75 – 89% at the corresponding concentrations ranging from 245 ± 101 copies/mL to (2.9 ± 0.5) x 10^6 copies/mL. In HIV patient samples, the repeatability was observed to be 59 – 78% at the corresponding concentrations ranging from 481 ± 73 copies/mL to 3910 ± 400 copies/mL.

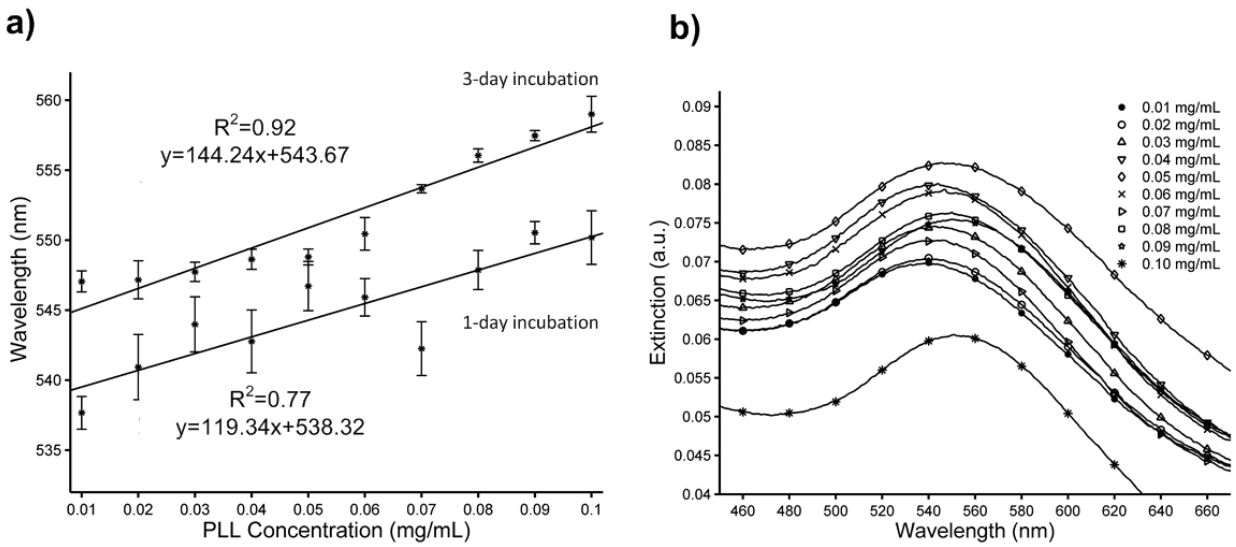

FIGURE S1. Surface modification of polystyrene surfaces and spectral peak shifts corresponding to varying poly-l-lysine (PLL) concentrations. a) To evaluate PLL concentration effect, gold nanoparticles were immobilized at various PLL concentrations onto polystyrene surfaces. A linear correlation was observed between the PLL concentration and the wavelength shift for the surfaces prepared by 1-day and 3-day incubation steps. For each data point, the nanoplasmonic wavelength peak was determined as the wavelength at the maximum extinction value analyzed with curve fitting method, and all data for wavelength measurements were presented as the mean of wavelength measurements ± standard error of the mean (SEM). b) Wavelength peak shifts by gold nanoparticle immobilization at PLL concentrations ranging from 0.01 to 0.1 mg/mL were evaluated using a 1-day PLL incubation step. The curves shown for each concentration were obtained by averaging all the plots at that concentration (n=5-6). For the following modifications, we used 0.05 mg/mL of PLL, since it has a high extinction intensity at this PLL concentration to maximize gold nanoparticle binding onto the PLL treated surface.

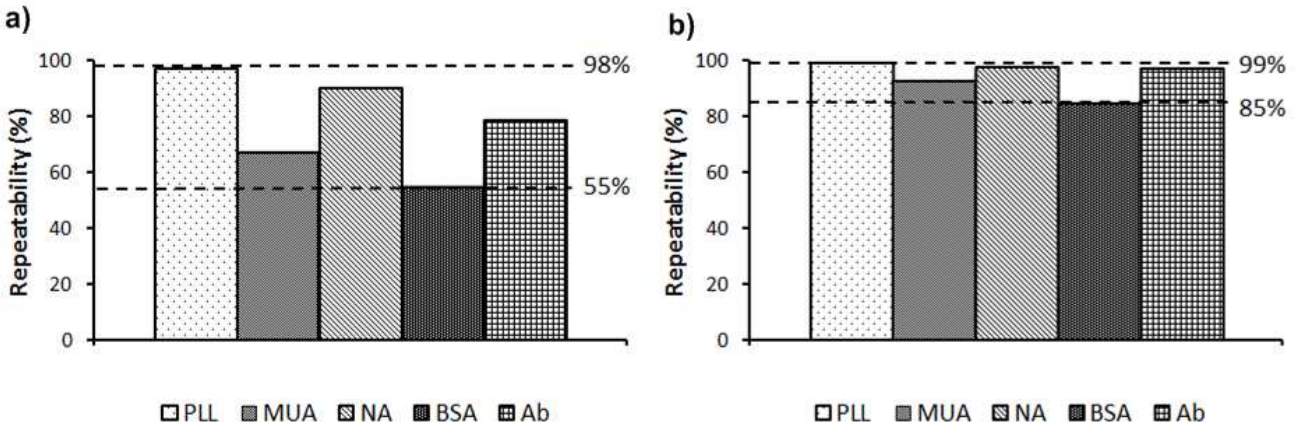

FIGURE S2. Reproducibility and repeatability of surface chemistry for nanoplasmonic platform. a) Repeatability parameter was evaluated for the wavelength shifts in each surface chemistry step. Overall, the repeatability parameter was observed to be 55 – 98% for wavelength measurements (n=6-216 for each surface chemistry). b) Repeatability parameter was evaluated for the extinction intensity measurements in each surface chemistry step. Overall, the repeatability parameter was observed to be 85 – 99% for extinction intensity measurements (n=6-216 for each surface chemistry).

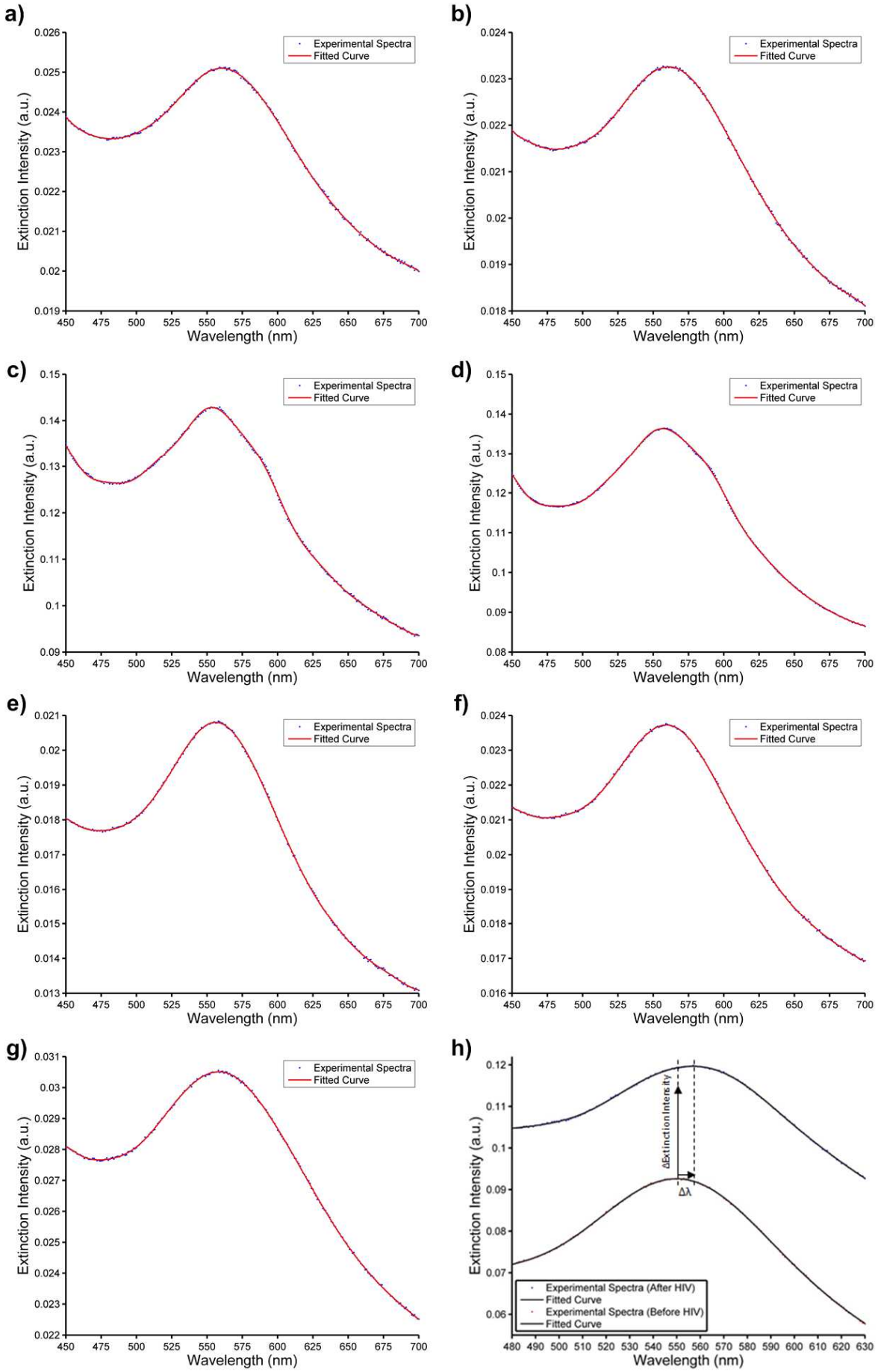
a)
b)
c)
d)
e)
f)
g)
h)
Experimental Spectra
Fitted Curve
Extinction Intensity (a.u.)
Wavelength (nm)
ΔExtinction Intensity
Δλ
Experimental Spectra (After HIV)
Fitted Curve
Experimental Spectra (Before HIV)
Fitted Curve

FIGURE S3. The curve fitting algorithm described in the Materials and Methods section was performed to fit to the experimental spectra. The analytical curve fits and the original experimental data were shown for representative spectra of HIV in spiked whole blood samples. a) Whole blood was spiked with HIV at (6.5 ± 0.6) x 10^5 copies/mL for subtype A, b) (8.3 ± 1.3) x 10^5 copies/mL for subtype B, c) (1.3 ± 0.2) x 10^6 copies/mL for subtype C, d) (3.8 ± 1.2) x 10^6 copies/mL for subtype D, e) (1.3 ± 0.2) x 10^6 copies/mL for subtype E, f) (1.1 ± 0.3) x 10^6 copies/mL for subtype G, and g) (2.9 ± 0.5) x 10^6 copies/mL for panel h) Representative plot of wavelength and extinction intensity shifts after the application of HIV to the biosensing platform. The arrows indicate the nanoplasmonic shifts due to subtype G detection as representative plot, when (9.3 ± 0.7) x 10^4 copies/mL HIV spiked in whole blood is applied.

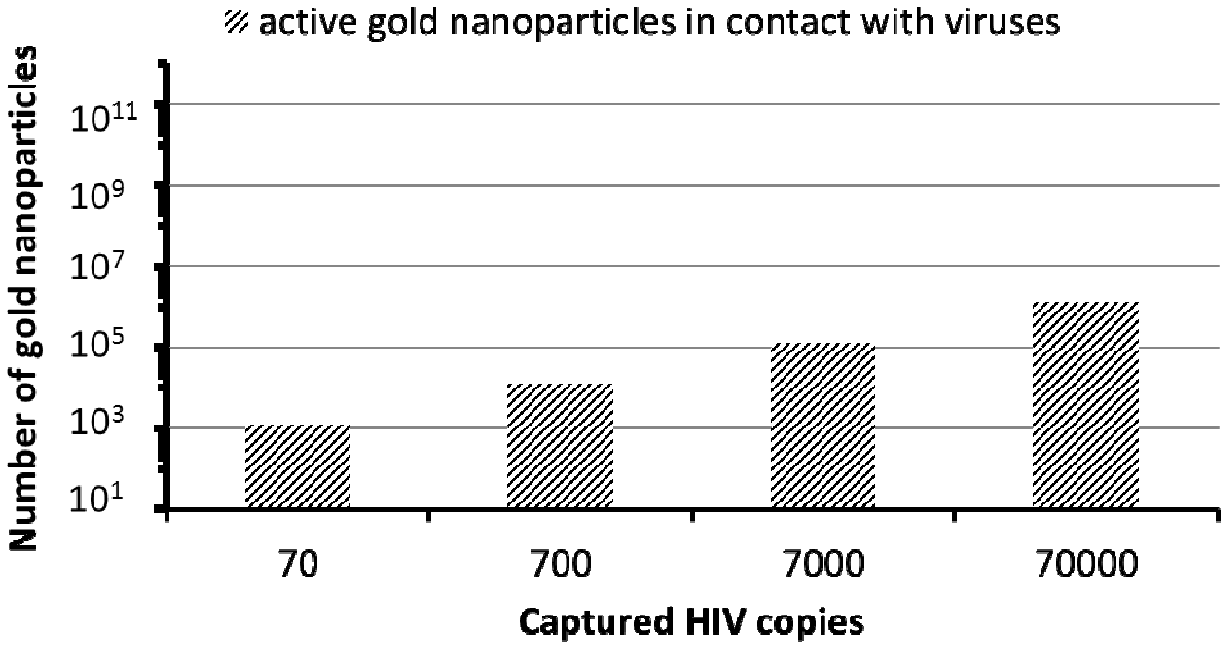

FIGURE S4. Number of total gold nanoparticles and active gold nanoparticles in contact with viruses are plotted as a function of captured HIV copies. For instance, for 100 HIV copies per mL, the model estimated that 70 HIV copies were captured out of 100 HIV copies suspended in 0.1 mL suspension. These captured 70 HIV copies interacted with 5436 gold nanoparticles, and 1340 of them were detected in the active area of the light beam. The captured HIV particles on biosensing surface were also visualized using Scanning Electron Microscopy, and the experimental images of the capture viruses were presented in Figure 3 in the manuscript.

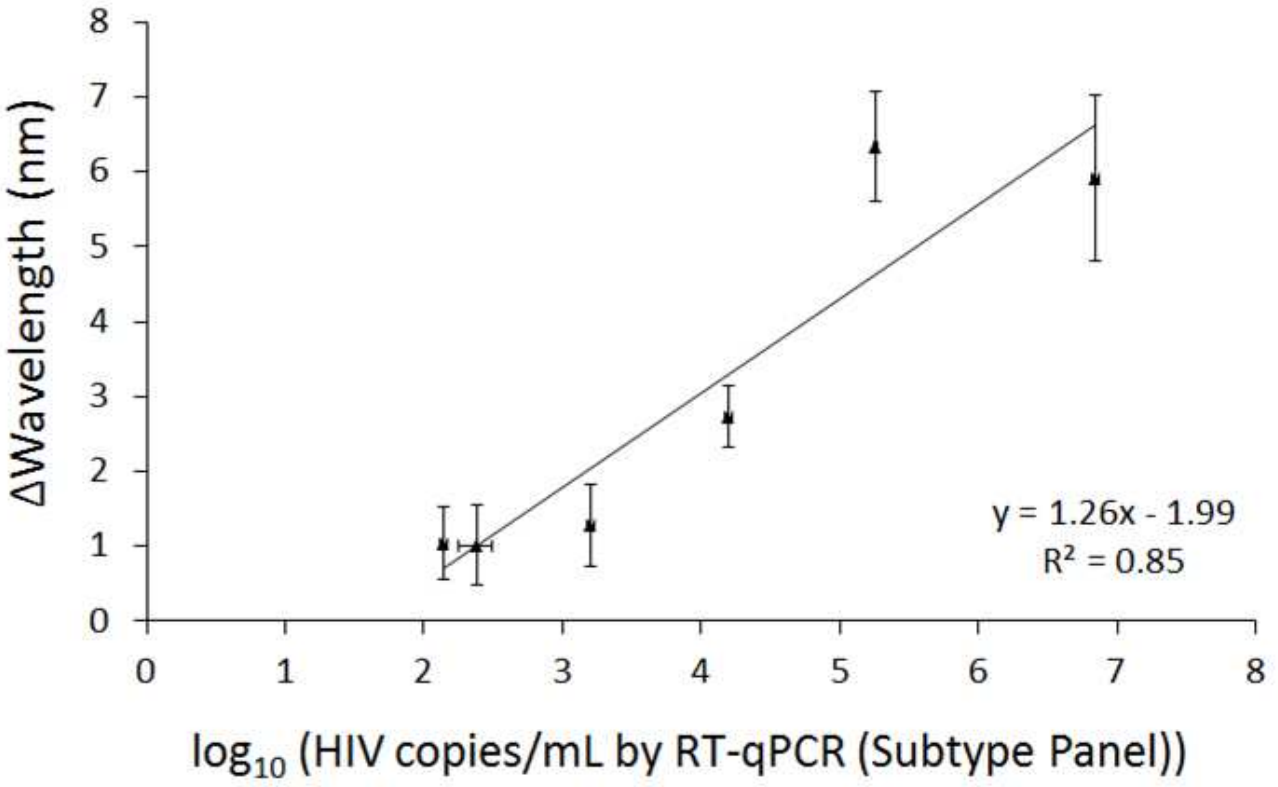

FIGURE S5. Validation of HIV subtype panel suspension in phosphate buffered saline (PBS) analyzed with the curve fitting method. HIV subtype panel in PBS was evaluated and observed that there was 5.9 ± 1.1 nm wavelength shift at (7 ± 0.4) x 10^6 copies/mL. The peak shift decreased to 1.0 ± 0.5 nm when the lowest concentration (138 ± 10 copies/mL) sample was used. The data for wavelength measurements were presented as wavelength measurements ± standard error of the mean (SEM) (n=6, error bars represent SEM). We performed 3 replicates for RT-qPCR measurements and 6 replicates for nanoplasmonic measurements for all samples.

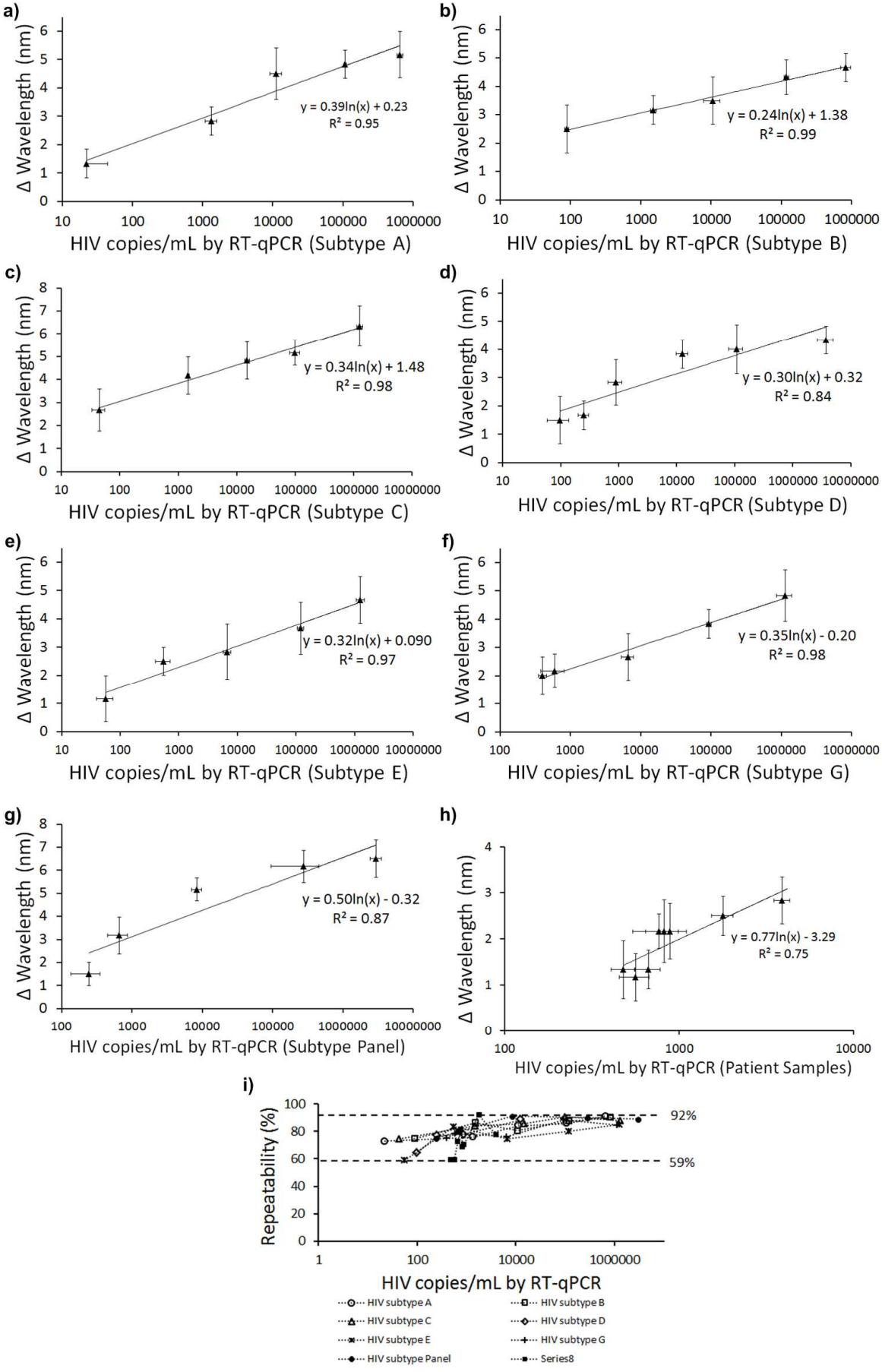
a)
Δ Wavelength (nm)
y = 0.39ln(x) + 0.23
R² = 0.95
HIV copies/mL by RT-qPCR (Subtype A)
b)
Δ Wavelength (nm)
y = 0.24ln(x) + 1.38
R² = 0.99
HIV copies/mL by RT-qPCR (Subtype B)
c)
Δ Wavelength (nm)
y = 0.34ln(x) + 1.48
R² = 0.98
HIV copies/mL by RT-qPCR (Subtype C)
d)
Δ Wavelength (nm)
y = 0.30ln(x) + 0.32
R² = 0.84
HIV copies/mL by RT-qPCR (Subtype D)
e)
Δ Wavelength (nm)
y = 0.32ln(x) + 0.090
R² = 0.97
HIV copies/mL by RT-qPCR (Subtype E)
f)
Δ Wavelength (nm)
y = 0.35ln(x) - 0.20
R² = 0.98
HIV copies/mL by RT-qPCR (Subtype G)
g)
Δ Wavelength (nm)
y = 0.50ln(x) - 0.32
R² = 0.87
HIV copies/mL by RT-qPCR (Subtype Panel)
h)
Δ Wavelength (nm)
y = 0.77ln(x) - 3.29
R² = 0.75
HIV copies/mL by RT-qPCR (Patient Samples)
i)
Repeatability (%)
92%
59%
HIV copies/mL by RT-qPCR
HIV subtype A
HIV subtype B
HIV subtype C
HIV subtype D
HIV subtype E
HIV subtype G
HIV subtype Panel
Series8

FIGURE S6. The validation with HIV spiked in whole blood and HIV-infected patient samples using experimental data maximum analysis method. a) HIV subtype A in whole blood led to 5.2 ± 0.5 nm wavelength shift at (6.5 ± 0.6) x 10^5 copies/mL. The peak shift was observed to be 1.3 ± 0.5 nm when ~50 copies/mL of HIV subtype A was used. b) (8.3 ± 1.3) x 10^5 copies/mL of HIV subtype B spiked in whole blood samples led to a wavelength shift of 4.7 ± 0.5 nm. The peak shift decreased to 2.5 ± 0.8 nm, when 89 ± 6 copies/mL HIV concentration was evaluated. c) For sampling with HIV subtype C in whole blood, (1.3 ± 0.2) x 10^6 copies/mL concentration was evaluated and the peak shift was observed to be 6.3 ± 0.9 nm. At ~50 copies/mL concentration, 2.7 ± 0.9 nm wavelength shift was observed. d) (3.8 ± 1.2) x 10^6 copies/mL of HIV subtype D in whole blood sample resulted a wavelength shift of 4.3 ± 0.5 nm. At the lowest concentration (98 ± 39 copies/mL), 1.7 ± 0.5 nm wavelength shift was observed. e) HIV subtype E in whole blood was evaluated and observed that there was 4.7 ± 0.8 nm wavelength shift at (1.3 ± 0.2) x 10^6 copies/mL. The peak shift decreased to 1.2 ± 0.8 nm when ~50 copies/mL of HIV subtype E was used. f) For sampling with HIV subtype G in whole blood, (1.1 ± 0.3) x 10^6 copies/mL concentration was evaluated and the peak shift was observed to be 4.8 ± 0.9 nm. At 404 ± 54 copies/mL concentration, 2.0 ± 0.7 nm wavelength shift was observed. g) HIV subtype panel in whole blood was evaluated and observed that there was 6.5 ± 0.8 nm wavelength shift at ((2.9 ± 0.5) x 10^6 copies/mL. The peak shift decreased to 1.5 ± 0.5 nm when the lowest concentration (245 ± 101 copies/mL) sample was used. h) Discarded HIV patient samples in whole blood were evaluated and observed that there was 2.8 ± 0.5 nm wavelength shift at 3910 ± 400 copies/mL. The peak shift decreased to 1.3 ± 0.6 nm when the lowest concentration (481 ± 73 copies/mL) sample was evaluated. i) Repeatability parameter was evaluated for the wavelength shifts for multiple HIV subtypes at various concentrations. Overall, the repeatability parameter was observed to be 59 – 92% for a broad range of concentrations for multiple HIV spiked and discarded HIV patient samples. The data for wavelength measurements were presented as wavelength measurements ± standard error of the mean (SEM) (n=4-6, error bars represent SEM). The viral load values were obtained by RT-qPCR and repeated at least 3

times each sample for each concentration.

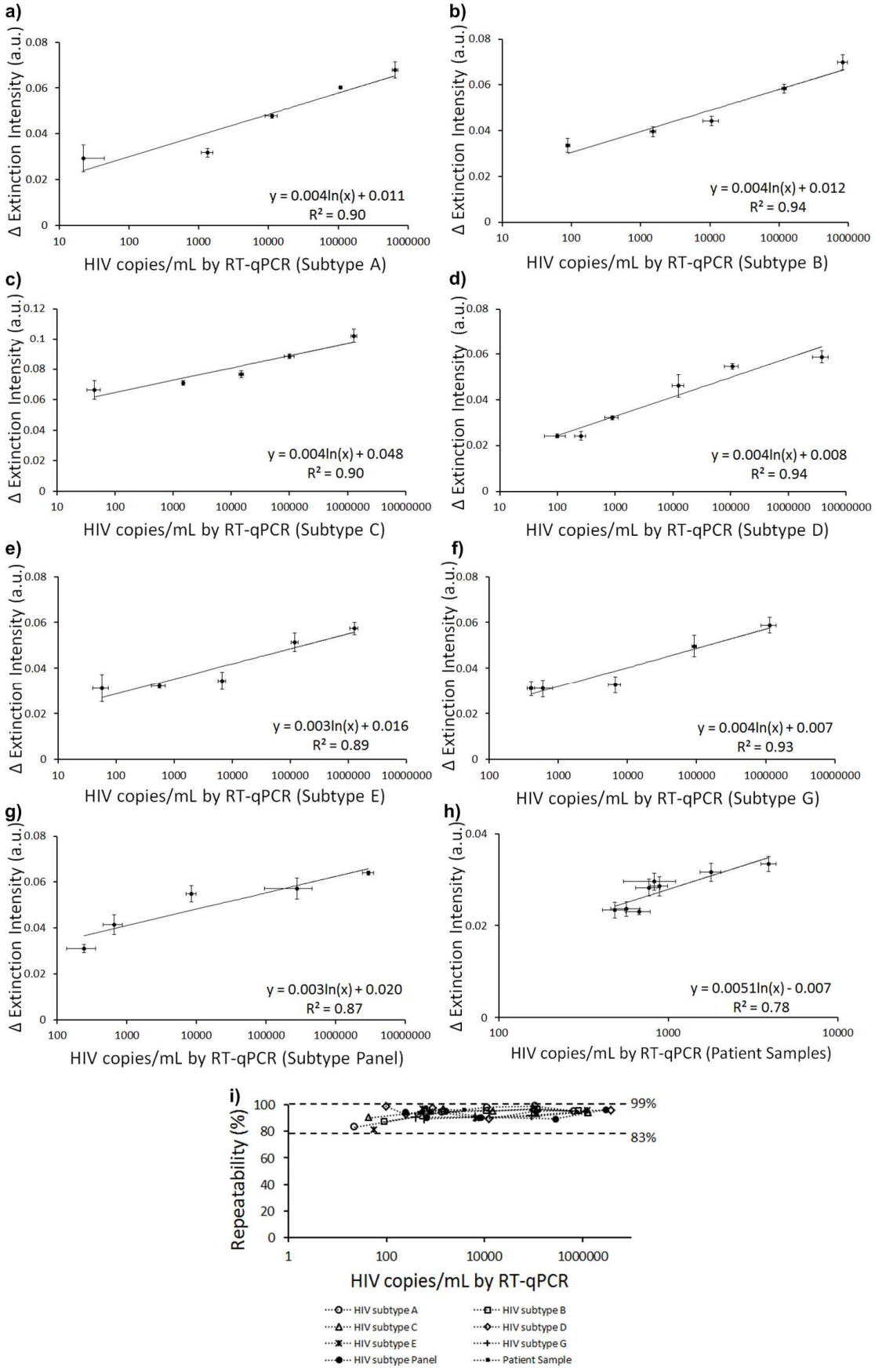
a)
Δ Extinction Intensity (a.u.)
y = 0.004ln(x) + 0.011
R² = 0.90
HIV copies/mL by RT-qPCR (Subtype A)
b)
Δ Extinction Intensity (a.u.)
y = 0.004ln(x) + 0.012
R² = 0.94
HIV copies/mL by RT-qPCR (Subtype B)
c)
Δ Extinction Intensity (a.u.)
y = 0.004ln(x) + 0.048
R² = 0.90
HIV copies/mL by RT-qPCR (Subtype C)
d)
Δ Extinction Intensity (a.u.)
y = 0.004ln(x) + 0.008
R² = 0.94
HIV copies/mL by RT-qPCR (Subtype D)
e)
Δ Extinction Intensity (a.u.)
y = 0.003ln(x) + 0.016
R² = 0.89
HIV copies/mL by RT-qPCR (Subtype E)
f)
Δ Extinction Intensity (a.u.)
y = 0.004ln(x) + 0.007
R² = 0.93
HIV copies/mL by RT-qPCR (Subtype G)
g)
Δ Extinction Intensity (a.u.)
y = 0.003ln(x) + 0.020
R² = 0.87
HIV copies/mL by RT-qPCR (Subtype Panel)
h)
Δ Extinction Intensity (a.u.)
y = 0.0051ln(x) - 0.007
R² = 0.78
HIV copies/mL by RT-qPCR (Patient Samples)
i)
Repeatability (%)
99%
83%
HIV copies/mL by RT-qPCR
HIV subtype A
HIV subtype B
HIV subtype C
HIV subtype D
HIV subtype E
HIV subtype G
HIV subtype Panel
Patient Sample

FIGURE S7. The validation with HIV spiked in whole blood and HIV-infected patient samples using extinction intensity variations analyzed with the experimental data maximum method. a) HIV subtype A in whole blood led to 0.068 ± 0.004 a.u. extinction intensity shift at (6.5 ± 0.6) x 10^5 copies/mL. The extinction intensity shift was observed to be 0.029 ± 0.006 a.u. when ~50 copies/mL of HIV subtype A was used. b) (8.3 ± 1.3) x 10^5 copies/mL copies/mL of HIV subtype B spiked in whole blood samples led to an extinction intensity shift of 0.070 ± 0.003 a.u. The extinction intensity shift decreased to 0.033 ± 0.003 a.u., when 89 ± 6 copies/mL HIV concentration was evaluated. c) For sampling with HIV subtype C in whole blood, (1.3 ± 0.2) x 10^6 copies/mL concentration was evaluated and the extinction intensity shift was observed to be 0.102 ± 0.005 a.u. At ~50 copies/mL concentration, 0.066 ± 0.006 a.u. extinction intensity shift was observed. d) (3.8 ± 1.2) x 10^6 copies/mL of HIV subtype D in whole blood sample resulted in an extinction intensity shift of 0.059 ± 0.003 a.u. At the lowest concentration (98 ± 39 copies/mL), 0.025 ± 0.003 a.u. extinction intensity shift was observed. e) HIV subtype E in whole blood was evaluated and observed that there was 0.057 ± 0.003 a.u. extinction intensity shift at (1.3 ± 0.2) x 10^6 copies/mL. The extinction intensity shift decreased to 0.031 ± 0.006 a.u. when ~50 copies/mL of HIV subtype E was used. f) For sampling with HIV subtype G in whole blood, (1.1 ± 0.3) x 10^6 copies/mL concentration was evaluated and the extinction intensity shift was observed to be 0.059 ± 0.003 a.u. At 404 ± 54 copies/mL concentration, 0.031 ± 0.007 a.u. extinction intensity shift was observed. g) HIV subtype panel in whole blood was evaluated and observed that there was 0.064 ± 0.003 a.u. extinction intensity change at (2.9 ± 0.5) x 10^6 copies/mL. The extinction intensity shift decreased to 0.032 ± 0.003 a.u. when the lowest concentration (245 ± 101 copies/mL) sample was used. h) Discarded HIV patient samples in whole blood were evaluated and observed that there was 0.033 ± 0.003 a.u. extinction intensity shift at 3910 ± 400 copies/mL. The extinction intensity shift decreased to 0.023 ± 0.003 a.u. when the lowest concentration (481 ± 73 copies/mL) sample was evaluated. i) Repeatability parameter was evaluated for the extinction intensity shifts for multiple HIV subtypes at various concentrations. Overall, the repeatability parameter was observed to be 83 – 99% for a broad

range of concentrations for multiple HIV spiked blood and discarded HIV-infected patient samples. The data for intensity measurements were presented as intensity measurements ± standard error of the mean (SEM) (n=4-6, error bars represent SEM). The viral load values were obtained by RT-qPCR and repeated at least 3 times each sample for each concentration.

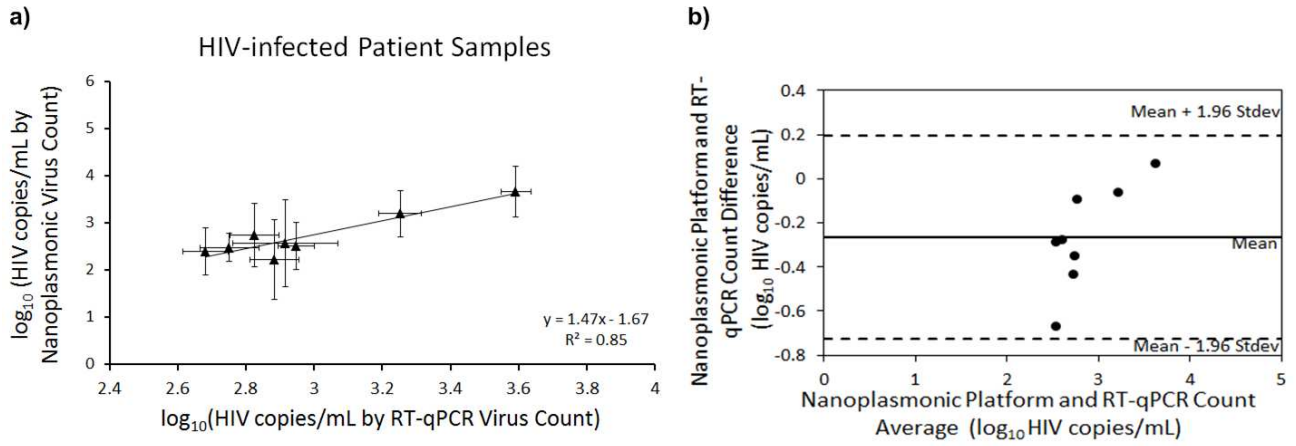

FIGURE S8. Quantitative detection with HIV-infected patient samples using extinction intensity measurements analyzed with the curve fitting method. a) Discarded HIV-infected patient samples in whole blood were evaluated using nanoplasmonic platform. Correlation was presented between HIV count obtained by RT-qPCR and nanoplasmonic platform. Nanoplasmonic platform presented a viral load ranging from (2.2 ± 0.9) $\log_{10}$ copies/mL to (3.7 ± 0.5) $\log_{10}$ copies/mL in patient samples. RT-qPCR count presented a viral load ranging from (2.7 ± 0.1) $\log_{10}$ copies/mL to (3.6 ± 0.1) $\log_{10}$ copies/mL copies/mL in patient samples. The data for wavelength measurements were presented as wavelength measurements ± standard error of the mean (SEM). (n=5-6, error bars represent SEM). b) Bland-Altman Analysis between the nanoplasmonic platform and RT-qPCR counts did not display an evidence for a systematic bias for HIV viral load for HIV-infected patient blood samples tested.

TABLE S1. Corresponding wavelength data for each PLL concentration evaluated with the curve fitting analysis method and incubation time.

Poly-l-lysine	3-day Incubation		1-day Incubation	
Concentration (mg/mL)	Nanoplasmonic Wavelenght (nm)	SEM	Nanoplasmonic Wavelenght (nm)	SEM
0.01	547.1	0.8	537.7	1.2
0.02	547.2	1.4	540.9	2.3
0.03	547.7	0.7	544.0	2.0
0.04	548.6	0.7	542.8	2.2
0.05	548.8	0.6	546.7	1.8
0.06	550.5	1.2	545.9	1.3
0.07	553.7	0.3	542.3	1.9
0.08	556.1	0.5	547.9	1.4
0.09	557.5	0.4	550.5	0.8
0.10	559.0	1.3	550.2	1.9

Abbreviations: SEM (standard error of the mean).

TABLE S2. Statistical significance (p-values) obtained using non-parametric Kruskal-Wallis one-way analysis of variance followed by Mann-Whitney U test with Bonferroni correction for multiple comparisons for the results obtained by experimental data maximum analysis of surface modification experiments.

	p-value
AuNP-PLL	0.01
MUA-NA	0.01
NA-BSA	0.19
BSA-Ab	0.01
Ab-Control	0.33

Abbreviations: AuNP (Gold Nanoparticle), PLL (Poly-L-Lysine), MUA (11-Mercaptoundecanoic acid), NA (NeutrAvidin), BSA (Bovine Serum Albumin), and Ab (Antibody).

TABLE S3. Statistical significance (p-values) obtained using non-parametric Kruskal-Wallis one-way analysis of variance followed by Mann-Whitney U test with Bonferroni correction for multiple comparisons for the results obtained by experimental data maximum analysis of whole blood (control) and multiple HIV subtypes experiments.

	p-value
Control - Subtype A	0.001
Control - Subtype B	0.001
Control - Subtype C	0.001
Control - Subtype D	0.001
Control - Subtype E	0.001
Control - Subtype G	0.001
Control - Subtype Panel	0.001

TABLE S4. Statistical significance (p-values) obtained using non-parametric Kruskal-Wallis one-way analysis of variance followed by Mann-Whitney U test with Bonferroni correction for multiple comparisons for root mean square (RMS) roughness of modified surfaces.

	p-value
PS - PLL	0.83
PS - AuNP	0.003
PLL - AuNP	0.003

Abbreviations: PS (Polystyrene), PLL (Poly-L-Lysine), and AuNP (Gold Nanoparticle).

TABLE S5. Parameters used in the model for capture of viruses.

Abbreviation	Definition	Value
V	volume of virus solution (mL)	0.1
C	number of copies of viruses per mL	$50 - 10^6$
A_b	optical beam area (mm^2)	3.14
A	surface area of wells (mm^2)	36.941
P	capture efficiency of viruses (%)	> 70
r	radius of a gold nanoparticle (nm)	5
λ	characteristic length of the ligand-receptor bonds (nm)	0.1
δ_{eq}	equilibrium separation distance between a virus and the surface (nm)	5
k_b	Boltzmann constant (J/K)	1.381×10^{-23}
a , R	half-length of major axis of virus (nm)	$50 - 100$
b	half-length of minor axis of virus (nm)	$50 - 100$
h_0	maximum distance at which ligand-receptor bonds can be formed (nm)	10
γ	virus aspect ratio ($=a/b$)	1
T	Temperature (K)	300

TABLE S6. Results of viral load analysis for 8 HIV-infected patient samples using nanoplasmonic biosensing platform and RT-qPCR.

Patient #	**RT-qPCR Count (Mean ± SEM) (log_{10} copies/mL)**	**Nanoplasmonic Count (Mean ± SEM) (log_{10} copies/mL)**
I	3.6 ± 0.1	4.3 ± 1.2
II	3.3 ± 0.1	3.3 ± 0.9
III	2.9 ± 0.2	2.2 ± 1.1
IV	2.8 ± 0.1	2.6 ± 1.2
V	2.7 ± 0.1	2.0 ± 0.8
VI	3.0 ± 0.1	2.0 ± 0.8
VII	2.8 ± 0.1	2.5 ± 1.0
VIII	2.9 ± 0.1	1.3 ± 0.7

Abbreviations: SEM (standard error of the mean).

REFERENCES

1. Sainsbury, T.; Ikuno, T.; Okawa, D.; Pacile, D.; Frechet, J. M. J.; Zettl, A., Self-assembly of Gold Nanoparticles at the Surface of Amine- and Thiol-functionalized Boron Nitride Nanotubes. *J. Phys. Chem. C* 2007, 111, 12992-12999.
2. Wang, S.; Esfahani, M.; Gurkan, U. A.; Inci, F.; Kuritzkes, D. R.; Demirci, U., Efficient On-Chip Isolation of HIV Subtypes. *Lab Chip* 2012, 12, 1508-1515.
3. Manak, M.; Sina, S.; Anekella, B.; Hewlett, I.; Sanders-Buell, E.; Ragupathy, V.; Kim, J.; Vermeulen, M.; Stramer, S. L.; Sabino, E.; *et al.*, Pilot Studies for Development of an HIV Subtype Panel for Surveillance of Global Diversity. *AIDS Res. Hum. Retroviruses* 2012, 28, 594-606.
4. Decuzzi, P.; Ferrari, M., The Adhesive Strength of Non-spherical Particles Mediated by Specific Interactions. *Biomaterials* 2006, 27, 5307-5314.